RESEARCH ARTICLE

VOLCANICA

Including a pressure dependent relation between static and dynamic elastic moduli in a Finite Element deformation model of Grímsvötn Volcano, Iceland

Sonja H. M. Greiner *α,β,γ and Halldór Geirsson[α]

[α] Nordic Volcanological Center, Institute of Earth Sciences, University of Iceland, Reykjavík, Iceland.
[β] Department of Earth Sciences, Uppsala University, Uppsala, Sweden.
[γ] Center for Natural Hazard and Disaster Science, Uppsala/Stockholm/Karlstad, Sweden.

Abstract

Surface deformation is an important tool for studying active volcanoes. Numerical deformation models can consider irregular features like crustal heterogeneity and avoid biases due to oversimplification. Dynamic elastic moduli can be derived from seismic velocities, but the static moduli apply to deformation studies since strain amplitudes and time scales differ. There is however no commonly acknowledged relation between the two. We implemented a Finite Element deformation model for the Icelandic subglacial volcano Grímsvötn, including bedrock topography and a 3D elastic structure. Dynamic elastic moduli, derived from seismic tomography and density structures, were converted into static moduli via an empirical pressure-dependent relation. The model requires a deformation source at 3–4.5 km depth, and a co-eruptive pressure changes of 8–70 MPa to fit deformation observed during the 2011 eruption at Grímsvötn. Larger source depths compared to previous deformation studies show the importance of considering crustal heterogeneity and static moduli in deformation models.

Ágrip

Jarðskorpuhreyfingar eru mikilvæg aðferð til að rannsaka virk eldfjöll. Töluleg bútalíkön geta tekið tillit til breytilegra eðliseiginleika jarðskorpunnar og minnkað áhrif of einfaldra forsendna á niðurstöður. Svokallaða kvika fjaðurstuðla má reikna út frá mælingum á hraða jarðskálftabylgna, en stöðugir fjaðurstuðlar henta betur í jarðskorpuhreyfingalíkönum vegna lengri tímaskala hreyfinga miðað við jarðskjálftabylgjur. Það er þó ekki til einföld jafna til að breyta á milli kvikra og stöðugra fjaðurstuðla. Við settum upp bútalíkan af jarðskorpuhreyfingum við Grímsvötn, sem tekur tillit til landslags og breytileika fjaðurstuðla í þrívídd. Þrýstiháð samband er sett fram til að breyta á milli kvikra og stöðugra fjaðurstuðla. Notaðar eru hreyfingar samfara 2011 Grímsvatnaeldgosinu á GNSS stöðinni GFUM ásamt reiknilíkani okkar til að skorða kvikuhólf á 3-4.5 km dýpi með þrýstifall um 8-70 MPa, að gefnum forsendum um stærð kvikuhólfsins. Niðurstöður okkar varðandi dýpi kvikuhólfs undir Grímsvötnum er meira en kom út úr líkönum með einsleita fjaðurstuðla og sýna mikilvægi þess að taka tillit til breytileika fjaðurstuðla jarðskorpunnar í líkönum af jarðskorpuhreyfingum.

Keywords: Volcano deformation; Finite Element Method; Elastic moduli; Grimsvotn; Iceland; Crustal heterogeneity.

1 Introduction

Magma moving through the Earth's crust displaces the surrounding host rock and the associated surface deformation is an important source of information for research and monitoring at active volcanoes [e.g. Mogi 1958; Lisowski 2007]. The pattern and amplitude of surface deformation varies depending on e.g. the host rock rheology and mechanical properties, deformation source location and depth, its geometry, dimensions, and pressure or volume change [e.g. Masterlark 2007; Poppe et al. 2024].

The degree of heterogeneity and the form of the crustal structure and topography can vary greatly between individual volcanoes, so that their influences on surface deformation need to be evaluated for individual case studies. Both aspects have been successfully implemented using numerical methods, like the Finite Element method [e.g. Dieterich and Decker 1975; Trasatti et al. 2003; Trasatti et al. 2005; Masterlark 2007; Currenti et al. 2008; Hickey et al. 2015]. However, the mechanical properties of a material can to some degree depend on the method with which they were estimated [Heap et al. 2020]. While for example the dynamic elastic moduli are most commonly derived from seismic wave velocities [Cheng and Johnston 1981; Eissa and Kazi 1988; Fjær 2019; Heap et al. 2020], the so called static elastic moduli can be determined through direct stress-strain measurements [Cheng and Johnston 1981; Adelinet et al. 2010; Eggertsson et al. 2020] or by analyzing crustal deformation [Grapenthin et al. 2006], which are both associated with longer timescales and higher strains. At atmospheric pressure, the ratio of dynamic to static bulk moduli often ranges between 2 and 4 depending on the individual rock type [Simmons and Brace 1965; Link 1968] and decreases towards unity with increasing pressure [e.g. Cheng and Johnston 1981; Adelinet et al. 2010]. Although the difference between static and dynamic elastic moduli has been known for decades, there is no widely acknowledged mathematical relation between them [Zhang et al. 2024]. While dynamic elastic structures derived from seismic velocities provide valuable information on material contrasts within the crust, they overestimate crustal stiffness compared to the static moduli, which are more appropriate for slower deformation processes. The

* shmgreiner@hi.is

Submitted: 2024-05-08 | Accepted: 2024-10-15 | Published: 2024-12-12

Editor: J. Farquharson | Typesetter: J. Farquharson

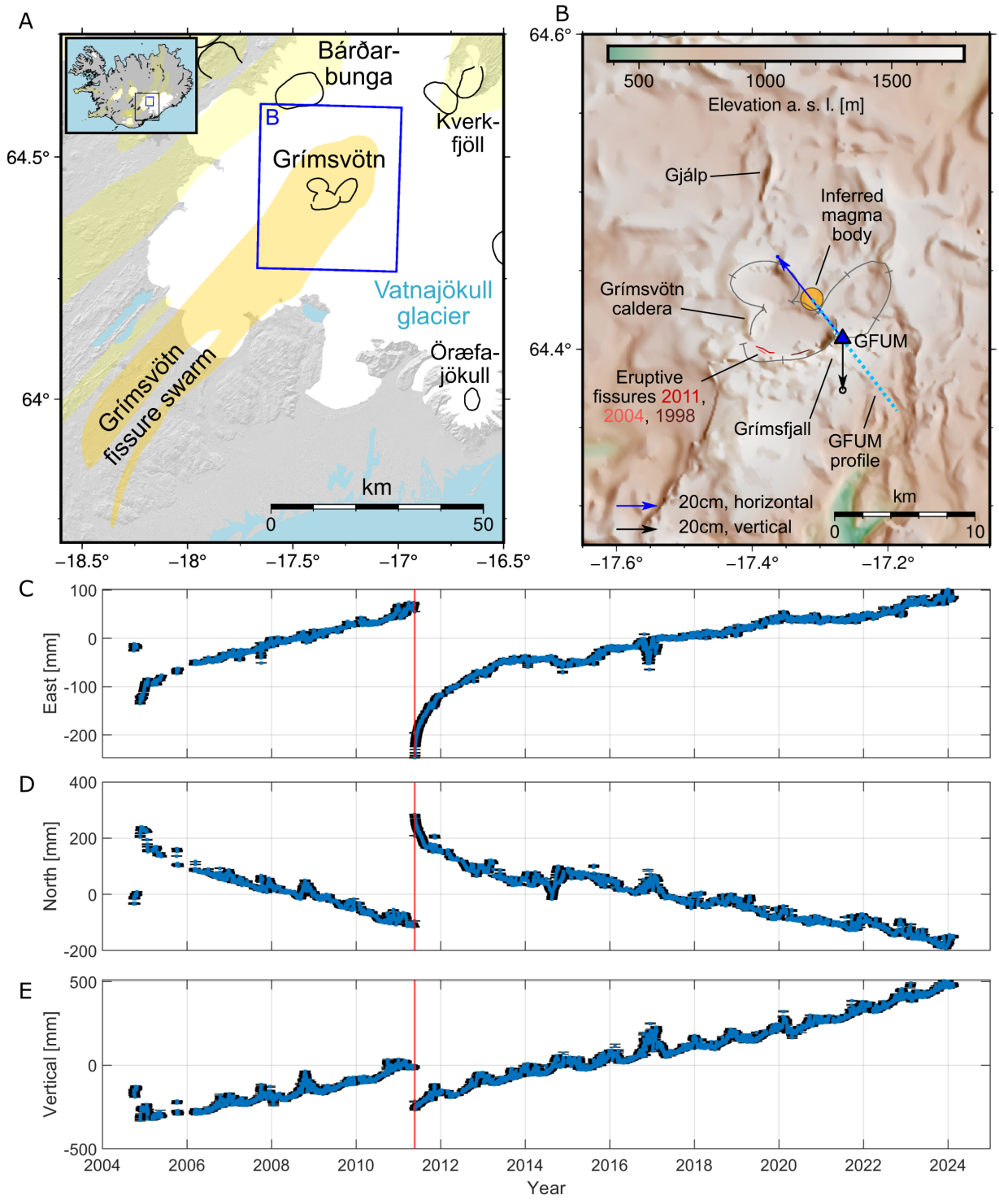

Figure 1: [A] Location of Grímsvötn and surrounding volcanic systems in central Southeast Iceland. Calderas (based on Einarsson and Sæmundsson 1987) are outlined in black, fissure swarms are colored yellow, apart from the Grímsvötn fissure swarm, which is marked in orange. White areas are covered by glacier. Blue rectangle marks outlines of [B]. Inlet: Iceland with locations of [A] and [B] marked by black and blue rectangles, respectively. [B] Surroundings of the Grímsvötn central volcano. Topographic relief corresponds to the subglacial bedrock [Gudmundsson 1989; Björnsson and Einarsson 1990; Gudmundsson et al. 1995; Magnússon 2008; Björnsson and Pálsson 2020]. Inferred location of shallow magma body based on Hreinsdóttir et al. [2014]. The triangle shows the location of GNSS station GFUM with co-eruptive displacement from 2011 [Hreinsdóttir et al. 2014]. The dotted blue line marks the profile, along which the deformation in this study is evaluated. [C]–[E] Time series of motion at GFUM relative to Eurasia. Red vertical lines mark the 2011 eruption. Data processed using `Gipsy-Oasis II` as described in Sigmundsson et al. [2022].

discrepancy caused by using dynamic rather than static moduli is often acknowledged as a potential source of uncertainty [Currenti et al. 2008; Hickey et al. 2015], but less frequently corrected for [Hickey et al. 2016; Gottsmann et al. 2020]. A pressure-dependent (i.e. depth-dependent) relation between the dynamic and static moduli was suggested by Wauthier et al. [2012], but they did not account for pressure-variations in their model and a pressure-dependent relation between dynamic and static moduli has not been fully applied to deformation models.

Although deformation models can provide constraints to source parameters, such as depth and pressure change, several studies find that the source pressure change especially often exceeds common failure criteria, e.g. the tensile strength of the host rock surrounding a magma reservoir [Trasatti et al. 2005; Masterlark 2007; Gudmundsson 2012; Hickey et al. 2015]. However, the pressure change can also be thought of as a proxy for volume change to drive deformation models. A magma body may expand through anelastic deformation or slight faulting. Therefore, magma chambers can grow in volume without significantly growing pressure [e.g. Sigmundsson et al. 2020b].

Here, we evaluate the influence of topography and an elastic 3D subsurface structure on surface deformation for the subglacial volcano Grímsvötn, Iceland, testing different magma reservoir geometries as deformation sources. We use a simple relation to convert the dynamic elastic moduli to the lower static moduli, which are used in forward 3D Finite Element deformation models. The predicted deformation is compared to coeruptive displacement from the 2011 eruption at Grímsvötn volcano.

2 Geological background of the Grímsvötn system

Iceland is an island in the North Atlantic, where the divergent plate boundary between the North American and Eurasian plates coincides with a mantle plume [e.g. Einarsson 2008; Sigmundsson et al. 2020a]. The plate boundary crosses Iceland approximately from southwest to northeast with volcanic systems distributed along it (inlet in Figure 1A).

2.1 The Grímsvötn Volcanic System

The Grímsvötn volcanic system, whose center is located underneath the western part of the Vatnajökull glacier (Figure 1A), extends tens of kilometers towards SSW and NNE. Among eruptions occurring on the fissure swarms is the Laki eruption from 1783–84 [Thordarson and Self 1993]. The central part of the volcanic system typically produces basaltic eruptions, which tend to be phreatomagmatic in nature due to interaction with the overlying glacier [Haddadi et al. 2017]. The name Grímsvötn will hereafter refer to the central volcano only, which is the focus of this study, rather than the entire system.

A research station with a continuously recording GNSS station (GFUM), a tiltmeter and a seismometer [Hreinsdóttir et al. 2014] is located on the northeastern part of a nunatak called Grímsfjall, which forms the southern rim of the largest of three overlapping calderas (Figure 1B). Due to the otherwise extensive glacial coverage, the station on Grímsfjall is the most important tool to observe nearfield surface deformation both during eruptions and in intereruptive periods [Sturkell et al. 2003; Vogfjörd et al. 2005; Hreinsdóttir et al. 2014; Reverso et al. 2014].

Surface deformation at GFUM shows consistent northwestward motion towards the caldera during eruptions, and in the opposite direction in intereruptive periods. There is little variation in the directions of motion between different eruptive cycles [Reverso et al. 2014]. This consistency in the directions of motion was interpreted as intereruptive inflation and coeruptive deflation of a spatially stable deformation source throughout the last three eruptive cycles [Hreinsdóttir et al. 2014; Reverso et al. 2014].

Gravitational and magnetic surveys revealed a shallow low-density body underneath the main caldera surrounded by dense structures interpreted as cone sheets or ring-dikes as well as a large, high-density, non-magnetic structure, that was interpreted as a large, slowly cooling intrusion [Gudmundsson and Milsom 1997]. These features were also found by a seismic tomography study by Alfaro et al. [2007]. A range of studies attempted to constrain the location, especially the depth of a magma reservoir at Grímsvötn and they can be grouped into studies finding shallow ($d < 7$ km) or deep ($d > 10$ km) reservoirs, or a combination of both (see Table 1).

The caldera hosts a subglacial lake, which empties in irregular intervals causing glacial outburst floods. In the past, some of these floods have been immediately followed by eruptions, as was last observed in 2004 [Vogfjörd et al. 2005; Albino et al. 2010]. This sensitivity and potential for interaction between the lake and a shallow magma reservoir emphasize the importance of studying the shallow magmatic plumbing system at Grímsvötn.

2.2 The 2011 eruption at Grímsvötn

The models implemented in our study are compared to coeruptive surface deformation of the Grímsvötn eruption in 2011. It was the largest eruption the system experienced since 1873, started in the evening of the 21st of May and lasted until the 28th of May [Hreinsdóttir et al. 2014; Haddadi et al. 2017]. It occurred on the southwestern edge of the main caldera (Figure 1B), which is notably not in the line of motion observed at GFUM. The cGNSS station GFUM and the accompanying tiltmeter, which were the only means to observe nearfield surface deformation at the time, recorded continuously throughout the eruption.

Although the eruption lasted for a week, the maximum coeruptive displacement was recorded within the first two days. After this, the direction of motion reversed, which was interpreted as slight recharge of the shallow reservoir by Hreinsdóttir et al. [2014] despite the ongoing eruption.

3 Methods

3.1 Geodetic data from the 2011 Grímsvötn eruption

The maximum coeruptive displacement recorded at GFUM during the 2011 eruption is $u_z = 253 \pm 10$ mm of subsidence and $u_r = 513 \pm 4$ mm of horizontal motion in the direction of

Table 1: Previous estimates of the depth and geometry of a magma body at Grímsvötn based on previous studies. Note that the depth refers to the central depth of each magmatic body.

Study	Method/Data	Geometry	Depth [km]
Gudmundsson and Milsom [1997]	gravity and magnetic survey	-	2
Sturkell et al. [2003]	GNSS (1998 eruption)	sphere	> 1.6
Alfaro et al. [2007]	seismic tomography	stock	3–7
Hreinsdóttir et al. [2014]	GNSS (2011 eruption)	sphere	1.7 ± 0.2
Reverso et al. [2014]	GNSS (2000–2012)	two vertically stacked penny-shaped cracks	shallow: 3; deep: 10–35
Haddadi et al. [2017]	thermobarometry	-	15 ± 5

Table 2: Model parameters by Hreinsdóttir et al. [2014] for the 2011 coeruptive deformation (GFUM and the tiltmeter) assuming a pressurized point source, a Young's modulus of E = 30 GPa and a Poisson's ratio of ν = 0.25.

Parameter	Value
Latitude	64.431–64.433°N
Longitude	17.310–17.314°W
Depth d	(1.7 ± 0.2) km
Volume change ΔV	(0.038 ± 0.004) km^3
Horizontal distance from GFUM r	(3.5 ± 0.2) km

N38.4 ± 0.5°W. The tiltmeter recorded δ = 175 ± 6 µrad along N35 ± 6°W [Hreinsdóttir et al. 2014]. The coeruptive direction of motion is similar to that of the previous two eruptions and opposite to the motion during intereruptive periods [Reverso et al. 2014]. The consistency of the direction of motion, which is offset from the eruptive vents of the last three eruptions, was interpreted as an indicator of a spatially fixed deformation source [Hreinsdóttir et al. 2014; Reverso et al. 2014]. Assuming that the direction of motion pointed directly towards the location of the center of the inferred magma chamber, Hreinsdóttir et al. [2014] used the maximum coeruptive displacement of the 2011 eruption to invert for the deformation source location, depth and strength parameter/volume change, using the Mogi model [Mogi 1958]. These model parameters as well as the assumed elastic parameters are listed in Table 2.

3.2 Model Setup

All models in this study were implemented using the Finite-Element software `COMSOL Multiphysics 5.6`. Further analysis was done in `MATLAB`. We implemented three configurations of models, adding topography and an elastic subsurface structure to a basic model individually and combined. The first model replaced the flat surface with topography and the second assumed a flat surface, but replaced the homogeneous material properties with a 3D elastic structure. The third and final set of models was a combination of the previous two. For some models, we kept the spherical pressurized cavity as the deformation source using the parameters listed in Table 2 to evaluate the effects of adding crustal heterogeneity. For other models, different source geometries were placed as pressurized cavities centered at the location suggested by Hreinsdóttir et al. [2014]. The source depth and pressure change of these models were manually varied to reproduce the co-eruptive displacement observed at GFUM during the 2011 eruption. The dimensions of the individually tested pressure sources were fixed a-priori to reduce the number of model parameters compared (Table 3). All numerical models are listed with key characteristics and source geometry in Table 4. Effects of gravity are not considered in this study. However, even without considering gravitational effects, topography may affect surface displacement, since the free surface is at variable elevation above the deformation source. Furthermore, the irregular and partially tilted surface may affect how stresses are distributed within the crust.

Table 3: Dimensions of the magma bodies tested as the deformation sources. All geometries are centred at 64.432°N, 17.312°W [Hreinsdóttir et al. 2014], i.e. at a distance of 3.56 km from GFUM. Penny-shaped cracks and the triaxial ellipsoid are aligned horizontally and semiaxes a, b, and c are aligned East-West, North-South and vertical, respectively. The source depth and pressure changes were chosen for each source so that the coeruptive displacement from 2011 at GFUM was reproduced by the models.

Geometry	Source dimensions [m]
Sphere (small)	a = 800
Sphere (large)	a = 1500
Penny-shaped crack	$a = b$ = 2000, c = 250
Triaxial ellipsoid	a = 3500, b = 2000, c = 500
2 vertically stacked penny-shaped cracks	$a_1 = b_1$ = 2000, c_1 = 250; $a_2 = b_2$ = 2200, c_2 = 500; $r_{conduit}$ = 30

All models in this study are purely elastic and therefore, reversible. For simplicity, all deformation and applied pressure changes are therefore assumed to be positive, which can be understood as absolute values. Visco- or poroelastic rheologies are assumed to be irrelevant since the deformation occurred on the timescale of a few days only. Plastic and brittle deformation possibly contributed to observed motion, but were neglected here. Future studies should however include more complex rheologies.

Table 4: List of all models in this study. See Table 3 for dimensions of deformation sources. If the depth/pressure change were kept fixed ("fix" in column 5) they were equal to d = 1.7 km and ΔP = 280 MPa, otherwise they were varied to match observed deformation ("var"). The "heterogeneous" subsurface refers to models which use the full 3D heterogeneous elastic structure including 3D variations in seismic velocity and density as well as the converted static moduli and a layer of hyaloclastite at the top.

Model	Surface	Subsurface	Source geometry	Depth & pressure change fixed/variable	Results plotted in Figure
BM	flat	homogeneous	small sphere	fix	Supplementary Material*
TSSM	topography	homogeneous	small sphere	var	Figure 5
Tfix	topography	homogeneous	small sphere	fix	Figure 6
E1	flat	1D seism. vel.	small sphere	fix	Figure 6
E2	flat	like E1 + 3D seismic velocity	small sphere	fix	Figure 6
E3	flat	like E2 + 1D density	small sphere	fix	Figure 6
E4	flat	like E3 + lateral density variations	small sphere	fix	Figure 6
E5	flat	like E4 + static moduli	small sphere	fix	Figure 6
E6	flat	like E5 + hyaloclastite = heterogeneous	small sphere	fix	Figure 6
ESSM	flat	heterogeneous	small sphere	var	Figure 7
ESLA	flat	heterogeneous	large sphere	var	Figure 7
EPSC	flat	heterogeneous	penny-shaped crack	var	Figure 7
ETAX	flat	heterogeneous	triaxial ellipsoid	var	Figure 7
E2PC	flat	heterogeneous	2 stacked penny-shaped cracks	var	Figure 7
Cfix	topography	heterogeneous	small sphere	fix	Figure 6
CSSM	topography	heterogeneous	small sphere	var	Figure 8
CSLA	topography	heterogeneous	large sphere	var	Figure 8
CPSC	topography	heterogeneous	penny-shaped crack	var	Figure 8
CTAX	topography	heterogeneous	triaxial ellipsoid	var	Figure 8
C2PC	topography	heterogeneous	2 stacked penny-shaped cracks	var	Figure 8

* https://doi.org/10.5281/zenodo.13981084

3.2.1 *Base model*

The base model (BM) consisted of a single block of homogeneous elastic material measuring 170 × 170 × 40 km and was benchmarked against the McTigue model [McTigue 1987] using the `dMODELS` package [Battaglia et al. 2013] (see Supplementary Material* for more information).

The base model was set up using parameters by Hreinsdóttir et al. [2014] (Table 2). The source radius of a = 800 m and pressure change (ΔP = 280 MPa) were both derived from their source strength parameter. The two parameters are related and the values chosen here are a compromise to avoid a very large source radius (close to the source depth) and an even higher pressure change (required for a smaller source radius). For consistency with the results by Hreinsdóttir et al. [2014], the models will be compared to deformation predicted by the Mogi model [Mogi 1958].

For all models, the top surface was free, while the bottom boundary was fixed and the sides were constrained by a roller condition, allowing for boundary parallel motion only. The mesh for all models was set up with the highest resolution at the deformation source and on the surface above it. With increasing distance from the deformation source, the mesh became coarser with the lowest resolution at the edges of the model domain.

3.2.2 *Topography model*

The first of the more realistic models replaced the flat surface of the basic model with the bedrock topography in an area centered around the Grímsvötn caldera. The digital elevation model (DEM) is based on radio-echo sounding by Gudmundsson [1989]. Improvements to the DEM were made by Björnsson and Einarsson [1990], Gudmundsson et al. [1995], Magnússon [2008], and Björnsson and Pálsson [2020]. The DEM covers an area of 32 × 37.5 km^2 with a resolution of 50 m, which is only a small part of the model domain. For the rest of the model surface, the surface elevation was interpolated linearly from the edge of the DEM towards the edge of the domain (70 km away from the edge of the DEM), which had an elevation equal to the average elevation

*https://doi.org/10.5281/zenodo.13981084

of the DEM (1050 m a.s.l.). This approach was chosen to prevent or smooth out potential effects of the extrapolated topography. Boundary conditions and material properties were identical to those of the basic model. A spherical magma reservoir was placed near the center of the caldera complex as in Hreinsdóttir et al. [2014] (Table 2, Figure 1B). When comparing the results of the topography model to those of the half-space model, it is important to consider which elevation should be used as a reference for the depth of the magma body, i.e. which elevation corresponds to depth $d = 0$. In this study, the reference was chosen as the elevation of the bedrock surface above the inferred location of the magma body, at 1245 m a.s.l. Using the elevation above a magma chamber as a reference was also suggested by Cayol and Cornet [1998] and Trasatti et al. [2003]. Just as in the basic model, the magma body had a radius of 800 m and its (lateral) location was kept fixed, thus in model TSSM only the depth and pressure change were varied to fit the vertical and horizontal displacement observed at GFUM (3.6 km southeast of the source center; Figure 1B). Other source geometries (Table 3) were tested as well, but only spherical sources were able to reproduce the geodetic observations.

3.2.3 *Elastic structure models*

The second set of models assumed a flat surface, but replaced the homogeneous elastic properties of the basic model by a 3D heterogeneous elastic structure. The elastic structure was implemented in six steps (models E1–E6, see Table 4) and deformation was computed after each of them to evaluate how strong the influence of each step on surface deformation is. For this purpose, a spherical deformation source with a radius of 800 m was embedded into the crust at 1.7 km depth and set to experience a pressure change of 280 MPa, which in combination with the radius used, is (in the basic model) equivalent to the source strength parameter suggested by Hreinsdóttir et al. [2014].

For model E1, the first component of the elastic structure added was a depth-dependent p-wave velocity model based on km 80 of the ICEMELT refraction profile [Darbyshire et al. 1998] (assuming a constant density of $\rho = 2700$ kg m^{-3} and $v_P/v_S = 1.78$). Seismic velocities and the density relate to the Young's modulus E and the Poisson's ratio ν through

$$E_{dyn} = \rho v_s^2 \frac{3v_P^2 - 4v_s^2}{v_P^2 - v_S^2}, \tag{1}$$

$$\nu = \frac{v_P^2 - 2v_S^2}{2\left(v_P^2 - v_s^2\right)}. \tag{2}$$

Since ν is only dependent on the v_P/v_S-ratio, which is assumed constant at 1.78 [Darbyshire et al. 1998], $\nu \approx 0.27$.

In addition to depth-dependent seismic velocities, model E2 also considered lateral velocity variations in the immediate surroundings of Grímsvötn by including a 3D p-wave velocity model by Alfaro et al. [2007]. It covers an area of 32 × 45 km with depths ranging from 1 km a.s.l. to 6 km b.s.l.. The ratio of p- and s-wave velocities as well as the density remained the same as for the previous step.

The third added component, implemented in model E3, included a depth-dependent density model. The density model was initially formulated for Grímsvötn's neighbouring volcano, Bárðarbunga by Sigmundsson et al. [2020b] and covers the uppermost 15 km of the crust. However, since the models developed in this study reach deeper than 15 km b.s.l. we assumed 3150 kg m^{-3} at a depth of 40 km b.s.l. as suggested by Gudmundsson [2003] and interpolated linearly between this depth and the shallower depths based on Sigmundsson et al. [2020b].

For model E4, lateral density variations are added based on a gravity model by Gudmundsson and Milsom [1997]. The main features of their model were a large high-density-body at depth interpreted as a cooling intrusion and a low-density structure above, interpreted as caldera-infill, which is framed by thin high-density-structures along the caldera boundaries and which were interpreted as old ring-dikes. Assuming a broadly axisymmetric setup, the 2.5D model is extended into two nested cylinders with a common symmetry axis (the z-axis). The outer cylinder measures 6 km in radius, reaches from 1 km a.s.l. down to 4 km b.s.l. and has a density which is increased by 200 kg m^{-3} compared to the rest of the domain. The inner cylinder has a radius of 3.2 km, reaches down to 2 km b.s.l. and has a density which is 200 kg m^{-3} lower than that of the rest of the model domain at the same depth. The two cylinders are centered in such a way, that their interface aligns approximately with the northern cliff of Grímsfjall (see yellow line in Figure 2). As a result, the centre of both cylinders is slightly offset from the location of the magma body and the centre of the main caldera/caldera complex.

The fifth component of the elastic model converts the dynamic elastic moduli into static moduli and was added to model E5. No commonly acknowledged formulation of their relation exists, but it is known to be dependent on pressure, i.e. depth [Cheng and Johnston 1981], which was quantified for basaltic lavas from the Reykjanes Peninsula (southwest Iceland) by Adelinet et al. [2010]. Their results show that for undrained samples the ratio of the dynamic to the static bulk modulus is close to 3 at an effective pressure of 0 MPa and it decreases with increasing pressure until the two moduli become equal at approximately 130 MPa. The depth and pressure, at which the two moduli become equal are here referred to as z_{eq} and $p\left(z_{eq}\right)$, respectively. Due to the glacial cover and high geothermal activity around the caldera [Gudmundsson and Milsom 1997], saturated conditions are a reasonable assumption for the shallow crust at Grímsvötn. Since the Poisson ratio remains constant in the entire model domain (due to $v_P/v_S = const.$), the ratio of dynamic over static Young's moduli behaves the same as the ratio of bulk-moduli. We assume in this study that the ratio of the dynamic to the static moduli changes linearly from 3 at the surface to 1 at 130 MPa with increasing lithostatic pressure $p\left(z\right)$ as

$$\frac{E_{dyn}}{E_{stat}} = 3 - 2\frac{p\left(z\right)}{p\left(z_{eq}\right)}. \tag{3}$$

This relation ensures that the static Young's modulus is $\frac{1}{3}$ of the dynamic modulus at the surface and that they are equal at $z = z_{eq}$. The lithostatic pressure $p\left(z\right)$ is calculated using the

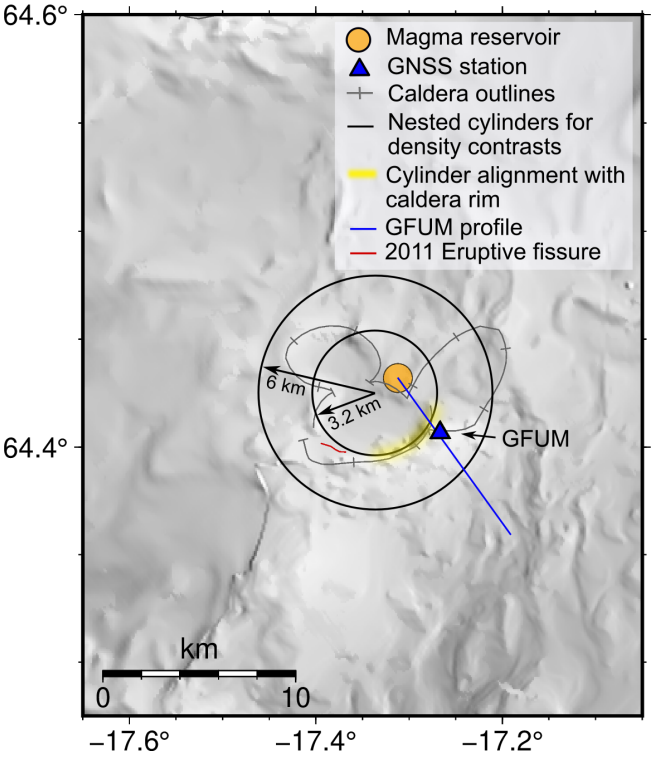

Figure 2: Position of the nested cylinders used to simulate lateral density variations under the main caldera. The yellow line marks the part of the northern cliff of Mt. Grímsfjall, which the cylinder interface was aligned with. The radius of the magma reservoir is a = 800 m. Note: The topography is shown here only to give a reference for the placement of the cylinders. It is not included in the elastic structure models, only in the combined models.

density models described earlier as

$$p\left(z_n\right) = g \sum_{i=2}^{n} \rho\left(z_i\right) \Delta z, \tag{4}$$

with $g = 9.81\ \mathrm{m\,s^{-2}}$, and a step-size $\Delta z = 10$ m and $p\left(z_1 = 0\right) = 0$ MPa (neglecting the presence of the glacier). Note that z is negative downwards and that both the density and the pressure increase with increasing depth. Equation 4 also allows to determine the depth z_{eq}, at which the static and dynamic moduli become equal. Technically, there are three different values found within the model domain: −3.9 km for everything apart from the main caldera, −3.6 km underneath the caldera walls and −4 km underneath the center. These three values differ due to the lateral density variations introduced in the previous model. However, considering that the uncertainty is likely higher than these differences, $z_{eq} = -3.9$ km was used for the entire model domain. The static moduli are therefore calculated as

$$E_{stat}\left(x,y,z\right) = \begin{cases} E_{dyn}\left(x,y,z\right) \cdot \frac{1}{3-2\frac{P(z)}{p(z_{eq})}} & z \geq z_{eq} \\ E_{dyn}\left(x,y,z\right) & z < z_{eq}, \end{cases} \tag{5}$$

with $z_{eq} = -3.9$ km and E_{dyn} according to Equation 1. A comparison between the static and dynamic moduli as functions of depths are shown in Figure 3 for the two different p-wave velocity models. A conceptually similar method to obtain static moduli was developed by Wauthier et al. [2012], also based on the results of Adelinet et al. [2010], but they used only a single value out of the entire structure.

The top of the material covered by the p-wave velocity structure by Alfaro et al. [2007] only reaches to 1 km a.s.l. but since significant parts of the central volcano are located at a higher elevation, an additional rock layer is added. Subglacial volcanism dominates near-surface geology, hence we use hyaloclastite material properties for this top layer in model E6. Hyaloclastite consists of magma that was fragmented to varying degrees due to contact with large amounts of water or ice and shows a wide range of elastic properties [Werner and Schmincke 1999; Watton et al. 2013; Eggertsson et al. 2020]. There is no quantitative information about the elastic properties of Grímsfjall, but Eggertsson et al. [2020] provided measurements of the Young's modulus of hyaloclastite at varying depths ranging from the surface down to ca. 700 m from the Krafla volcanic system in northern Iceland. Based on this, E was defined to range from 2.5 GPa at 1 km a.s.l. (where the underlying velocity model stops) to 0.8 GPa at 1.8 km a.s.l. (interpolated linearly). Note, that in the model with only the elastic subsurface structure (but no topography), the model surface was located at 1.4 km a.s.l. meaning that the lowest value for E was not reached. The values reported by [Eggertsson et al. 2020] are based on direct stress-strain-measurements, which means they are static values already and the static-dynamic

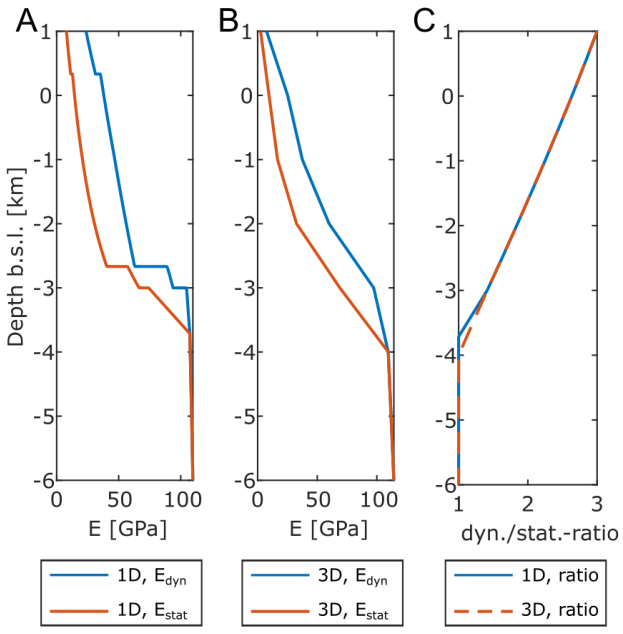

Figure 3: Static and dynamic Young's moduli in the shallow crust for [A] the 1D velocity structure by Darbyshire et al. [1998] and [B] the background of the 3D velocity structure (each depth is represented by a data point which is not affected by any velocity anomaly) by Alfaro et al. [2007] as well as [C] the ratio of dynamic over static Young's moduli for the respective datasets.

relation derived in the previous step was not applied to the hyaloclastite layer.

It is important to emphasize here, that the source parameters of models E1–E6 are identical, only the elastic subsurface structure is variable. The purpose of these models was not to reproduce motion observed at GFUM, but rather to test in what ways and by how much the individual elements making up the elastic subsurface structure affected surface deformation.

Furthermore, we tested five different magma chamber geometries (Table 3) to match the co-eruptive displacement observed at GFUM using the final heterogeneous elastic structure (models ESSM–E2PC; using the same subsurface structure as E6). These geometries are based on geometries and dimensions suggested by previous studies: spherical sources as an analogue to the Mogi model used by e.g. Hreinsdóttir et al. [2014] or Sturkell et al. [2003], the triaxial ellipsoid resembling the stock suggested by Alfaro et al. [2007] and the penny-shaped crack(s) after Reverso et al. [2014]. All sources were centered at the coordinates suggested by Hreinsdóttir et al. [2014] (see Table 2) and the only parameters which were altered in our models were the source depth d and the pressure change ΔP, which was applied evenly across the deformation source (neglecting effects such as buoyancy). If more parameters would have been left unconstrained, the model would be strongly underdetermined, as only data from a single GNSS-station and a tiltmeter are available for coeruptive deformation from the 2011 eruption. Of the two varied parameters, the depth was the only one that affected the ratio of horizontal to vertical surface deformation. Therefore, for each source geometry, we first adjusted the depth to match the observed ratio of 2.03 ± 0.09 and then adjusted the pressure change to match the observed deformation amplitudes.

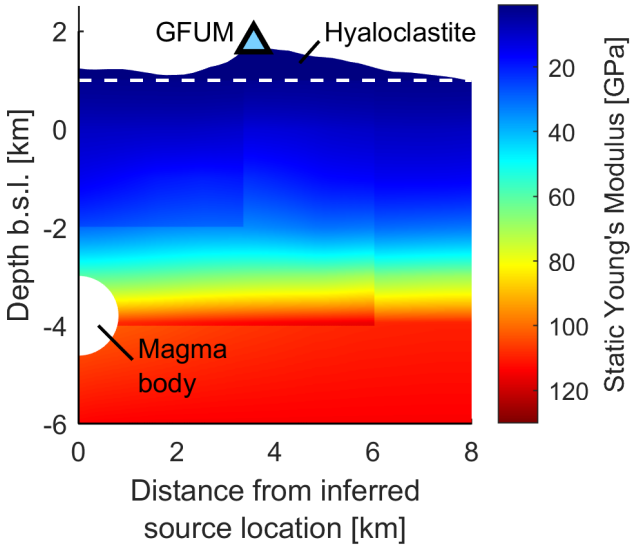

Figure 4: Cross-section through the crust along the GFUM profile showing the heterogeneous static Young's modulus ranging between 0.8 –130 GPa. The white dashed line marks the transition between moduli derived from seismic velocities (below) to values for hyaloclastite (above) based on Eggertsson et al. [2020]. In the elastic structure model (without topography), the hyaloclastite layer has a constant thickness of 400 m instead of the varying thickness shown here, but the underlying elastic structure is identical.

3.2.4 *Combined model*

The third and last set of models (CSSM–C2PC) combined models ESSM–E2PC with topography. As for models ESSM–E2PC, the depth and pressure were adjusted to match observed coeruptive displacement at GFUM. A cross section through the crust from the magma body along the profile through GFUM is shown in Figure 4. For consistency with models E1–E6, there is one additional model (Cfix) using the same source parameters as the base model and E1–E6, but with the full heterogeneous subsurface structure and topography.

4 Results

4.1 Topography

The horizontal and vertical components of deformation along the GFUM profile are very similar between the Mogi model and model TSSM (Figure 5A). For both components, the model with topography (TSSM) predicts slightly lower displacement within the caldera. The non-zero displacement in the horizontal component directly above the deformation source is a computational artifact of the mesh (no mesh node directly above the centre of the magma body). The most striking difference between the two models is found around the location of GFUM (ca. 3–4 km from the source), where the horizontal component of the topography model flattens out. Comparison to the bedrock elevation profile (Figure 5B) indicates that this stagnation coincides with the cliff at the northern face of Grímsfjall. Outside of the caldera (beyond Grímsfjall) the horizontal displacement predicted by TSSM is slightly larger than the prediction of the Mogi model. The azimuth changed slightly from 39° west of North to 36.6° west of North.

As the horizontal location of the source was fixed, only minor changes were necessary to fit the topography model, increasing the depth from 1.7 km to 1.8 km below the caldera floor and decreasing the pressure change from 280 MPa to 270 MPa.

4.2 Elastic structure

Two different approaches were taken to test the influence of the 3D elastic subsurface structure on deformation. At first, the same source parameters used for the basic model (depth, geometry, radius, pressure change; see Table 2) were used as input for models E1–E6 which incorporated the different elements of the elastic subsurface structure (Figure 6). This demonstrates which elements have a strong or weak influence on the resulting surface deformation. These models explicitly do not attempt to fit or reproduce observed deformation, but they rather attempt to show how much models with the same source parameters vary if the crustal properties change. The second set of models (ESSM–E2PC) tested five different source

geometries (Table 3) and compared them to the deformation observed at GFUM during the 2011 eruption (Figure 7). For these models, the depth and pressure change were modified to match the observed ground motion at GFUM.

The deformation predicted by models with increasingly complex elastic structures shows that adding the 1D seismic velocity (model E1) decreases the surface deformation (Figure 6A and 6B). Although the amplitudes of both components change, the vertical displacement is affected stronger than the horizontal component, which leads to an increase of the ratio of horizontal over vertical displacement (Figure 6D). Adding the 3D velocity model by Alfaro et al. [2007] in model E2 increases the deformation inside the caldera (left of the red line in Figure 6A–6C) significantly, although at GFUM mainly the horizontal component is affected. The addition of the two density models (models E3 and E4) has only minor effects. Noticeably, the abrupt material contrast introduced by the cylindrical bodies in model E4 is not reflected in the surface deformation. The strongest effect on the deformation is observed once the relation between the static and dynamic elastic moduli is considered in model E5. Figure 6D indicates that the horizontal component is more sensitive to this than the vertical. Lastly, the addition of the hyaloclastite in model E6 results in an increase of the amplitudes with the effect being almost equally strong in both components.

Although the five models with different source geometries (ESSM–E2PC) all reproduce the observations at GFUM within the uncertainty limits of the observations, the deformation varies elsewhere, especially within the caldera (Figure 7A and 7B) as do the depth and pressure changes required to fit the observations at GFUM (??). Compared to the Mogi model, all tested geometries result in lower displacement amplitudes inside the caldera (Figure 7A and 7B), reducing the vertical component by ~30–60 % above the source and the maximum horizontal displacement by ~30–50 %. The deepest sources (the two spherical reservoirs) experience the largest reduction in the nearfield but a broadening of the overall affected area. In the horizontal component (Figure 7A), the models with the triaxial and penny-shaped sources (ETAX and EPSC) behave clearly different from the spherical sources and the analytical model, even outside of the caldera. The vertical deformation (Figure 7B) indicates that there is hardly any difference between the models with the triaxial ellipsoid (ETAX) and the one with the two penny-shaped cracks (E2PC). Especially within the caldera, the two spherical sources produce differing displacement amplitudes despite being located at the same depth. In contrast to the analytical model, the ratio of horizontal over vertical displacement for all five models increases non-linearly with increasing distance from the deformation source. The unsymmetric sources (triaxial ellipsoid and penny-shaped cracks; EPSC, ETAX, E2PC) indicate faster increasing gradients than the spherical sources (ESSM, ESLA; Figure 7C).

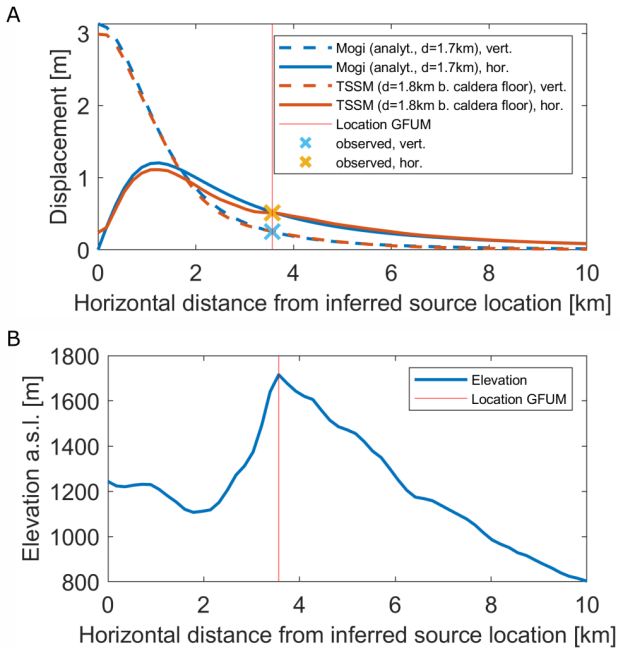

Figure 5: [A] Horizontal (solid) and vertical (dashed) component of deformation along the GFUM profile predicted by the analytical Mogi model (blue lines) and the numerical model with topography (TSSM; orange lines). Observed coeruptive displacement from GFUM is marked as "x" for both components. [B] Bedrock elevation along the profile with the part inside of the caldera on the left. Location of GFUM is marked in red in both figures.

The source depths we find for the different geometries vary between ca. 3.1–4.3 km below the bedrock surface (??). All of those values are significantly deeper than that of the analytical model. This is consistent with findings from previous studies, which have shown that considering crustal heterogeneities often changes source locations and especially increases their depth [e.g. Masterlark 2007; Foroozan et al. 2010; Hickey et al. 2016]. Pressure changes vary across almost three orders of magnitude, although the value for the smaller of the two spherical sources (ESSM), which had a radius of 800 m, has to be considered as highly unrealistic, because the pressure is far beyond the strength of the host-rock [e.g. Haimson and Rummel 1982; Currenti and Williams 2014], which leaves the pressure to vary between ca. 8–55 MPa for the other four sources. The lowest pressure change is required by the triaxial ellipsoid (model ETAX), which also is the shallowest of all tested sources. The azimuth of horizontal surface deformation is with 33° significantly lower than that for the other sources (42°). The volume change of the deformation source can be found by integrating over the displacement at the surface of the deformation source and we find values ranging between ca. 38–47 $\times$ 10^6 m^3 (??).

4.3 Combined model

All models combining the topography with the elastic subsurface structure (CSSM–C2PC in Table 4) were able to reproduce the observations from GFUM for the five tested geometries (Figure 8). Within the caldera, all models predict lower amplitudes of displacement than the analytical model in both components, with similar although slightly lower amplitudes to the elastic-structure models (ESSM–E2PC). Coinciding with the cliff at Grímsfjall, the horizontal component flattens out as

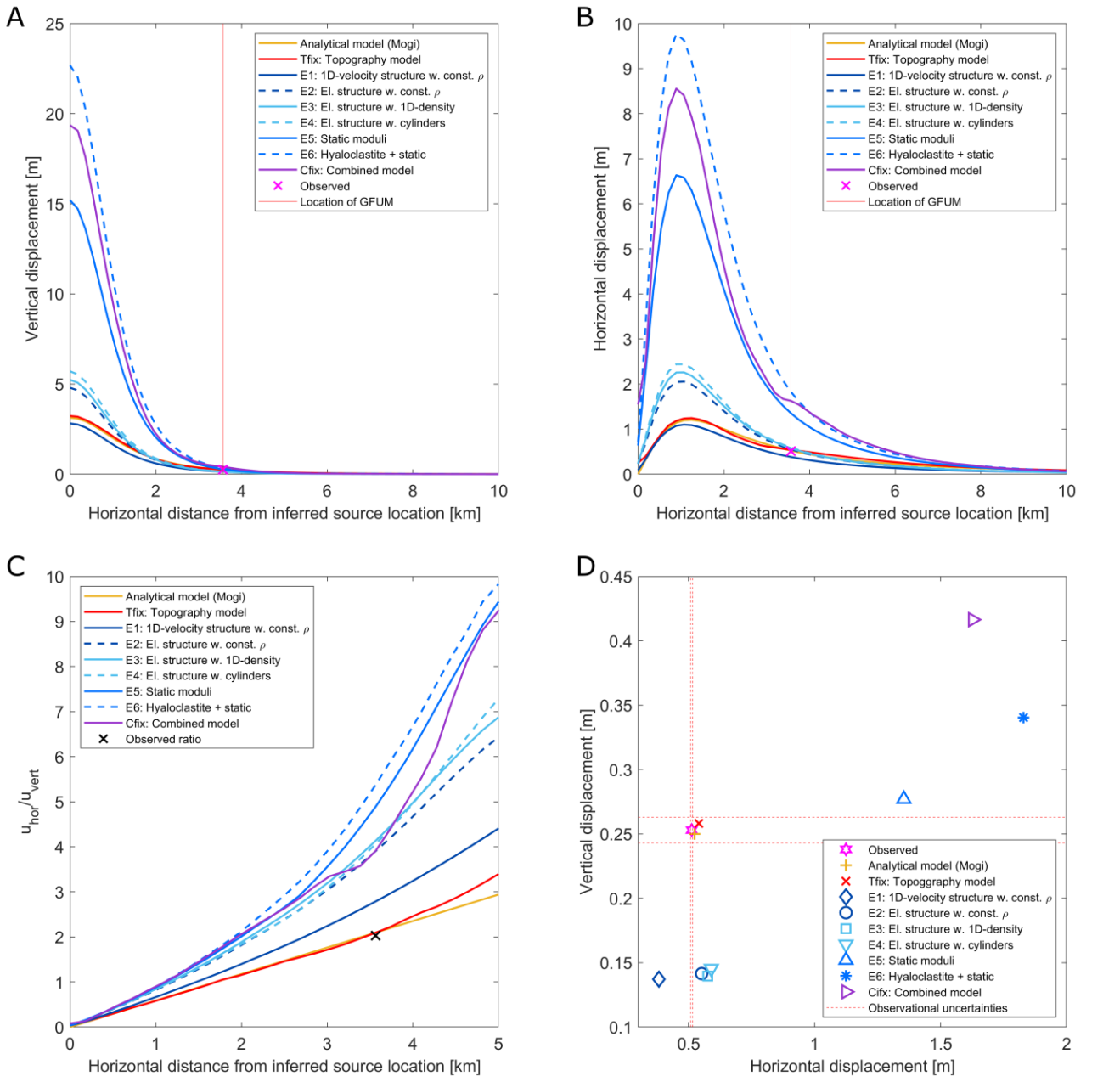

Figure 6: [A] Vertical and [B] horizontal surface deformation along the GFUM profile for a spherical magma body at 1.7 km depth (radius 800 m, ΔP = 280 MPa in elastic structures of successively increasing complexity; models E1–E6). [C] Ratio of horizontal to vertical displacement along the profile. [D] Displacement at cGNSS station GFUM. Location of the GFUM profile indicated in Figure 1B. The six blue lines/points in each figure correspond to the models E1–E6 (see Table 4). For reference, the analytical model, the topography model, and the combined model (models Tfix and Cfix, respectively; using the same model parameters) are also shown.

already observed in the topography model (TSSM; Figure 5A and Figure 8B), however this effect is much more pronounced when combined with the elastic subsurface structure.

The adjusted model parameters, d and ΔP are similar to the results for the elastic-structure models ESSM–E2PC (??). In the combined model, the spheres are located slightly deeper than in the previous model (comparing CSSM/CSLA to ESSM/ESLA), while the shallower sources (CPSC, CTAX, C2PC) required a slightly shallower depth compared to the model without the topography (EPSC, ETAX, E2PC). The pressure change ΔP changed slightly, increasing for the spheres (CSSM, CSLA) and very slightly for the penny-shaped crack (CPSC), decreasing for the triaxial ellipsoid and for the two vertically stacked penny-shaped cracks (CTAX, C2PC). The deformation source volume changed little between the elastic structure models (ESSM–E2PC) and the combined models (CSSM–C2PC), increasing or remaining constant for the spheres and slightly decreasing for the non-spherical mod-

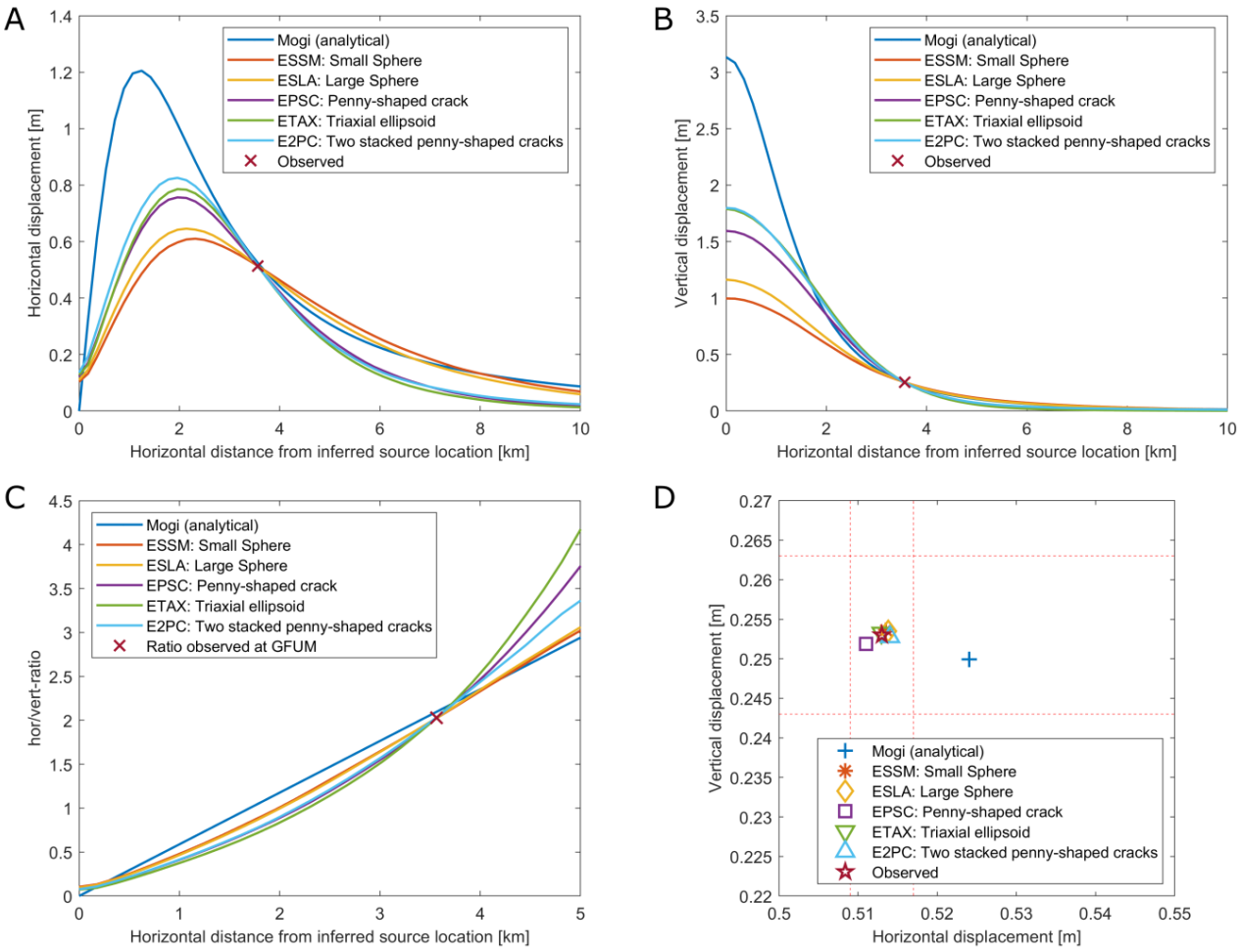

Figure 7: Elastic-structure models ESSM–E2PC (see Table 4 for model configurations). [A] Horizontal and [B] vertical deformation as well as [C] the ratio of horizontal to vertical displacement predicted by the elastic structure model and the analytical Mogi model along the profile through the inferred magma chamber location using different deformation source geometries. [D] Displacement at GFUM. The analytical model used the parameters reported by Hreinsdóttir et al. [2014], see Table 2, the source geometries and depth/pressure change for the numerical models are listed in Table 3 and ??, respectively.

els. The azimuth of the horizontal displacement at GFUM predicted for the different geometries (??) is lower for each geometry compared to the elastic-structure-only model by a small but consistent amount of 1–2°.

Table 5: Tilt predicted by the Mogi model and the combined model using the fits for the five different geometries listed in ?? at GFUM. The observed co-eruptive tilt was reported as δ_{obs} = 175±6 µrad [Hreinsdóttir et al. 2014].

Model	Geometry	δ [µrad]
Mogi (analytical)	point source	172
CSSM	small sphere	113
CSLA	large sphere	127
CPSC	penny-shaped crack	178
CTAX	triaxial ellipsoid	193
C2PC	2 penny-shaped cracks	184

An additional constraint or point of comparison between the models testing several geometries and the observational data is the tilt (Table 5). The best fit between the observations (δ_{obs} = 175 ± 6 µrad) is the model using the penny-shaped crack (CPSC). The spherical models do not fit the tilt well.

5 Discussion

5.1 Effects of topography

We find that the effects on surface deformation from considering topography in an otherwise homogeneous model (models TSSM and Tfix) were strongly localized to areas of comparatively steep slopes or cliffs, which is consistent with previous studies [Cayol and Cornet 1998; Williams and Wadge 1998; Trasatti et al. 2003; Masterlark 2007; Currenti et al. 2008; Hickey et al. 2015; Johnson et al. 2019]. In most deformation models with topography implemented for volcanic systems, such as at Etna, the topography adds material above the magma body and mainly affects vertical deformation [e.g.

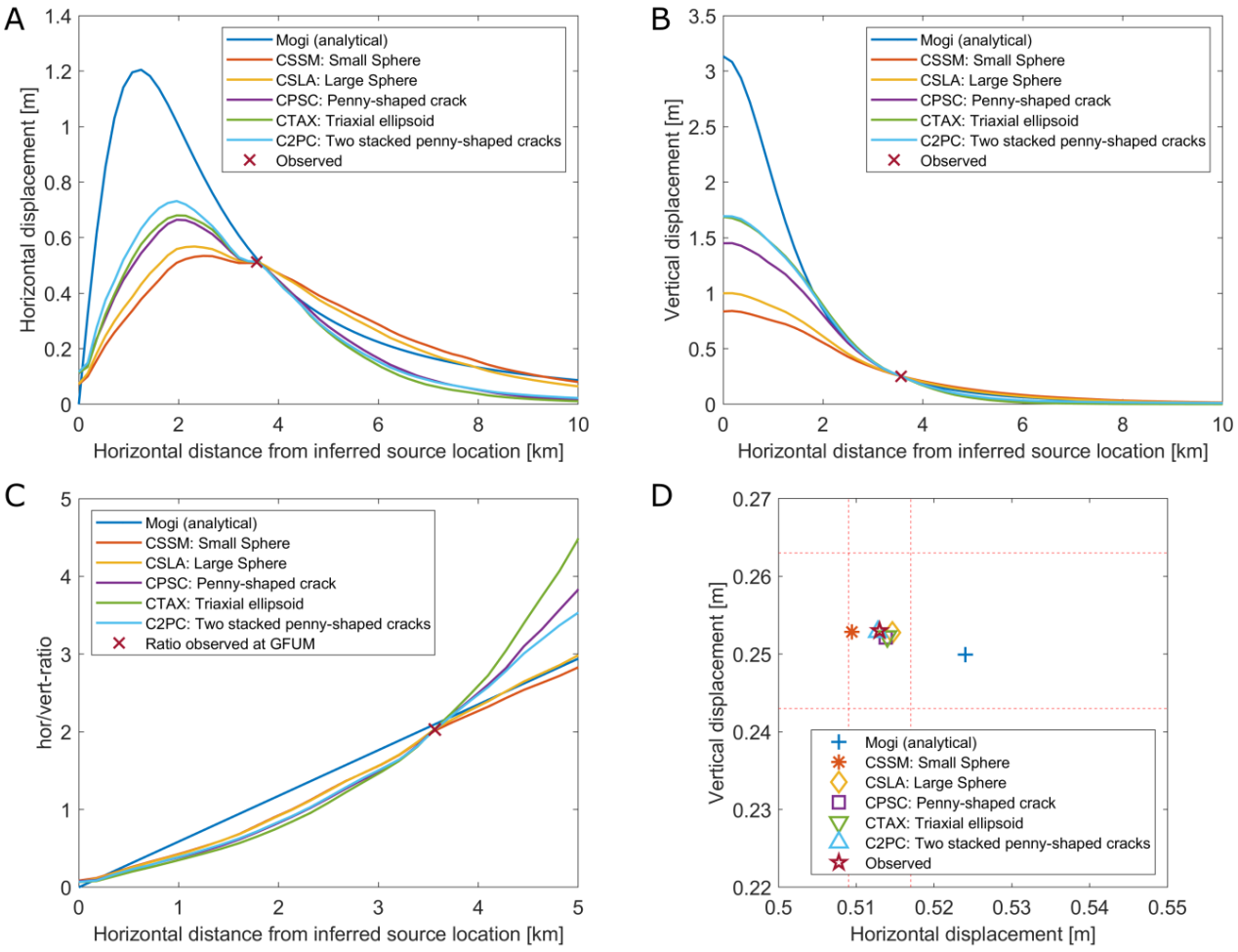

Figure 8: Combined models CSSM-C2P (see Table 4 for model configurations). [A] Vertical and [B] horizontal deformation and [C] the ratio of horizontal to vertical displacement predicted by the combined model and the analytical Mogi model along the profile through the inferred magma chamber location using different deformation source geometries. [D] Displacement at GFUM. The analytical model used the parameters reported by Hreinsdóttir et al. [2014], see Table 2, the source geometries and depth/pressure change for the numerical models are listed in Table 3 and ??, respectively.

Cayol and Cornet 1998; Williams and Wadge 1998; Trasatti et al. 2003; Currenti et al. 2008; Hickey et al. 2015]. In the present study, the bedrock surface above the inferred magma reservoir is at a lower elevation than GFUM, so there is a material deficit relative to the GNSS station, which is less frequently studied [Johnson et al. 2019]. Similar to Johnson et al. [2019], deformation at GFUM is oblique to the cliff, which may contribute to the clearly visible stagnation of the horizontal component (Figure 5, Figure 8) and affect the tilt. This emphasizes the importance of including the topography not only for stratovolcanoes, but also for systems with well-developed calderas and to further evaluate the influence of topography for monitoring stations close to cliffs and caldera rims. GFUM appears to be in a location with relatively mild topographic effects despite its proximity to the caldera rim. However, we cannot exclude that this is partially related to the resolution of the DEM, which was used to implement the topography. A higher resolution may lead to sharper changes in the topography and to more pronounced effects on deformation. However, no bedrock DEM with higher resolution is available for Grímsvötn at this time.

The influence of topography on the model parameters in model TSSM required to fit the observed deformation were minor. Even when comparing the source depth between the elastic structure models ESSM–E2PC and the combined model (CSSM–C2PC; heterogeneous crust), the depth did not vary by more than 300 m, which falls well within common estimates of uncertainties. The azimuth of the horizontal displacement changed slightly from 39° (Mogi model) to 36.6°, but both values are within the uncertainty of the 35 ± 6° recorded on the tiltmeter [Hreinsdóttir et al. 2014]. In conclusion, the topography at Grímsvötn has, for all models implemented here, a visible, but small effect.

5.2 Effects of crustal heterogeneity

The elastic structure has a much stronger influence on both the surface deformation pattern (e.g. Figure 6) and the model parameters when compared to topographic effects (??), which

is consistent with findings from previous studies [e.g. Trasatti et al. 2003; Masterlark 2007; Foroozan et al. 2010; Hautmann et al. 2010]. Based on the deformation profiles shown in Figure 6, the two aspects of the heterogeneous elastic structure with the largest influence on the predicted surface deformation are the 3D velocity model by Alfaro et al. [2007] and the consideration of the static instead of the dynamic elastic moduli, which result in an increase of surface deformation of a factor of ~2 and 3 in amplitude, respectively. In contrast to this, other elements caused changes on the order of a few, up to ~30 %. Seismic velocity models strongly affecting deformation models is a well known phenomenon [e.g. Hautmann et al. 2010; Hickey et al. 2015; Hickey et al. 2016; Gottsmann et al. 2020]. The density contrasts introduced by the nested cylinders have very little effect on deformation along the GFUM profile. It is however possible, that they would have more pronounced effects on model parameters in an inversion, which would be based on a more extensive monitoring network.

Applying a pressure-dependent ratio to connect the static and dynamic elastic moduli to a deformation model is a novel aspect of this study. A conceptually similar approach to obtain static moduli was suggested by Wauthier et al. [2012], but they did not account for variable pressure in their final model. Additionally, the values and ratios used in their study differ from those used in the present study. Although the confining pressure is not the only parameter influencing the relation between the two elastic moduli [Fjær 2019; Heap et al. 2020], it was deemed the most relevant here. Future studies could consider effects of additional parameters such as variable porosity [e.g. Got et al. 2019]. Heap et al. [2020] stated that applying estimates of static moduli from laboratory experiments directly to edifice-scale deformation models may lead to scaling issues due to the size of heterogeneities present on a volcano-scale, which cannot be present in a laboratory sample (e.g. macroscopic fractures). We anticipate that these scaling issues are mitigated to some degree in our study by two factors: 1) We do not not use direct estimates of the moduli from laboratory experiments but only their ratio. If both moduli are affected to a similar degree, these effects may cancel out. 2) We combined these laboratory estimates with data from seismic velocities, which should represent these large-scale heterogeneities to a larger degree than laboratory samples. However, effects of large fractures and faults on deformation are still not considered explicitly, but may directly affect surface deformation [e.g. Folch and Gottsmann 2006]. Overall, the average Young's modulus of the shallow crust is comparable to the effective large-scale estimate of 40 ± 15 GPa, which was suggested for Iceland based on seasonal deformation by Grapenthin et al. [2006].

The markedly peaked deformation within the caldera (Figure 6) indicates that the cylindrically shaped volume filling the caldera with a softer material, which is introduced both by the 3D seismic velocity model and the nested cylinders, acts as a kind of stress conduit, channeling stresses to propagate upwards rather than laterally. Unfortunately, the glacial cover in combination with the caldera lake at Grímsvötn make direct observations of ground deformation within the caldera currently impossible. However, a conceptually similar pattern of peaked deformation combined with increased source depths and reduced pressure changes (when compared to a homogeneous, elastic half space model) were also reported for Okmok volcano (Alaska) by Masterlark [2007] and Soufrière Hills Volcano, Montserrat [Hautmann et al. 2010]. It should be noted, that the introduction of the static moduli not only increased the contrast of elastic moduli between the surface and at depth, but also altered the gradient of the elastic moduli, which may further affect the stress distribution in the model. As already observed for the topography model, the horizontal displacement component of the combined models (CSSM–C2PC) seems to be more sensitive to topography than the vertical component. However, since the dimensions and lateral location of the deformation sources were kept fixed, the depth remained the only variable parameter affecting the ratio of horizontal over vertical displacement at a given distance from the magma body (in the present case: at GFUM), which for each geometry tested allowed the depth to be determined with some degree of uniqueness (??). The heterogeneous elastic subsurface-structure dominates the combined model (surface deformation and model parameters) and is in turn mostly influenced by the relation between static and dynamic moduli and the 3D p-wave velocity structure.

5.3 Source volume change

The volume changes of the deformation sources tested in this study range between 36–44 × 10^6 m^3 (models CSSM–C2PC), which is very similar to the estimates of 38 ± 4 × 10^6 m^3 and 35–43 × 10^6 m^3 found by Hreinsdóttir et al. [2014] from surface deformation. This is almost an order of magnitude lower than the erupted volume inferred from tephra fallout, which was estimated at 270 ± 70 × 10^6 m^3 by Hreinsdóttir et al. [2014].

The difference between deformation- and tephra-based volume change estimates could partially relate to host rock rigidity and magma compressability as suggested by Hreinsdóttir et al. [2014]. However, if compressibility alone were to explain this, the magma within the reservoir would need to be compressed by a factor of close to 10, which is on the upper end of what is typically considered for volcanic systems [Rivalta and Segall 2008; Anderson and Segall 2011]. Alternatively, the mismatch could indicate that there are neglected aspects of the crustal structure or processes, which significantly affect deformation. This could for example be related to co-eruptive feeding of magma into the shallow reservoir from a deeper source. The slight onset of inflation before the end of the 2011 eruption was observed by Hreinsdóttir et al. [2014], but not considered in their models or the present study. The repeated alignment of eruptive fissures with the caldera boundaries (Figure 1B) furthermore suggests that the feeder dike propagated along the caldera-bounding faults. Slip or dike opening along these faults is not considered in the present study or in the models by Hreinsdóttir et al. [2014]. If the caldera faults accommodated part of the coeruptive deformation, a GNSS station located outside of the caldera would underestimate deformation inside of the caldera and consequently, the coeruptive volume change [e.g. Amelung et al. 2000; Folch and Gottsmann 2006]. The potential influence of the caldera-bounding faults

at Grímsvötn was beyond the scope of this study, but should certainly be addressed in the future.

5.4 Implications for the Grímsvötn volcanic system

Our results constrain the source depth to range between ca. 3–4.5 km below the surface (1.8–3.5 km b.s.l.), which is significantly deeper than the 1.6–1.7 km suggested by some previous geodetic studies [Sturkell et al. 2003; Hreinsdóttir et al. 2014]. The model with the two vertically stacked penny-shaped cracks requires depths (using the combined model), which agree reasonably well with the parameters suggested by Reverso et al. [2014]. Additionally, the consideration of a deeper magma body agrees with geochemical results by Haddadi et al. [2017], which indicated a source significantly deeper than 2–3 km. Alfaro et al. [2007] noted the absence of earthquakes below ca. 2 km depth underneath the main caldera. This can be used as a constraint for minimum depth required for a magma body, which is fulfilled by all geometries tested, even when considering that the depth listed in ?? corresponds to the center of the magma body. The penny-shaped crack model (CPSC) is somewhat similar in depth to the one suggested by Albino et al. [2010].

The ratio of horizontal to vertical displacement, which was used here and in previous studies to determine the depth of the magma body, was significantly smaller (at GFUM/GRIM) for the eruptions in 1998 and 2004 compared to 2011 [Reverso et al. 2014]. Although this may to some degree relate to uncertainties in the data, the current model can only accommodate a single ratio for each magma body location. More complex pressure conditions in a more complex magma plumbing system would likely be a better representation of real systems [Cashman et al. 2017; Liao et al. 2018] and may be able to reproduce several ratios for different eruptions using a single source geometry. However, we focused here on a rather simple set of boundary conditions for the magma body itself since the primary focus of this study was the effect of the crust surrounding the reservoir.

The pressure changes required by the different geometries in the combined model (CSSM–C2PC) range from ~8 MPa up to >600 MPa with four out of five geometries ≤70 MPa. The models set up here assume a purely elastic crust and it is common for such models to predict unrealistically high pressure changes [Trasatti et al. 2005; Masterlark 2007; Hickey et al. 2015]. This is often one of their largest points of critique. However, deciding if a given pressure change is realistic is not always straightforward, since estimating the failure conditions around individual magmatic bodies depends among other factors on the body's geometry, tectonic setting, the failure mode, the host-rock-properties, and the method used to estimate them [Albino et al. 2010; Gudmundsson 2012; Currenti and Williams 2014]. Using Finite Element models and assuming shear failure to occur, Currenti and Williams [2014] found that an extensive tectonic setting, a non-spherical geometry, and steep topography are all factors which reduce the stresses, at which failure occurs. Given that Grímsvötn is located in an extensional setting, it would be expected to fail at low overpressure, which agrees with the volcano's high eruption frequency [Thordarson and Larsen 2007]. Additionally, the pressure changes required by the combined models (CSSM–C2PC) to fit the observation from GFUM decrease as the geometries move further away from that of a sphere with the triaxial ellipsoid (CTAX) requiring the lowest pressure change. At depth between 2–3 km, Currenti and Williams [2014] found that oblate sources failed at overpressures between 10–30 MPa, while spheres failed at up to 70 MPa. Considering these values, our results seem to be in an acceptable range, although it should be considered that Currenti and Williams [2014] used different material properties for their host-rock than the current study, which in turn influence the exact failure conditions. Alternative to model-based approaches, failure conditions can be estimated based on in-situ measurements from hydrofracturing experiments in boreholes [e.g. Haimson and Rummel 1982]. This method usually assumes tensile failure to occur and results in maximum possible overpressures of between ca. 0.5–9 MPa [Gudmundsson 2012]. Using these values, only the the triaxial ellipsoid (CTAX) has realistic values. Lastly, estimates of km-scale tensile strength based on InSAR data [Jónsson 2012] yield values of 1–3 MPa, which would leave all models with unrealistically high pressure changes. The upper limit for a realistic pressure change does not only depend on the host rock strength or failure conditions alone, but magma buoyancy and the potential formation of underpressure can also play a role [Gudmundsson et al. 2016; Sigmundsson et al. 2020b; 2024]. However, the magma reservoir at Grímsvötn is thought to be located at shallow depth, which limits effects of buoyancy and there are no indications for large motion along the caldera faults, as they were observed for example at Bárðarbunga in 2014 [Gudmundsson et al. 2016]. This suggests that if underpressure developed in the reservoir during the eruption, it must have been too small to initiate such motions. We therefore argue that this did not alter the possible pressure change by much more than 10–20 MPa at most [Sigmundsson et al. 2024], which would still leave many of the required pressure changes to be unrealistically high.

When comparing the results of the combined or elastic structure models (ESSM–E2PC and CSSM–C2PC) to the pressure changes required by homogeneous elastic models (the analytical Mogi model, BM, or TSSM), it appears as if the elastic structure reduced the pressure changes required to produce deformation of a similar amplitude (if keeping the source depth constant, see e.g. Figure 6). Especially considering the static rather than dynamic elastic moduli may help to reduce pressure changes required to fit surface deformation. Previous studies showed that considering inelastic deformation can further reduce the required pressure changes [e.g. Trasatti et al. 2005; Hickey et al. 2015].

One of the assumptions made to limit the number of model parameters was to keep the magma body's center fixed at 64.432 °N, 17.312 °W [Hreinsdóttir et al. 2014]. With this, the azimuth of four out of five geometries tested with the combined model was too large. Correcting this would probably require the magma body to be located slightly further to the east, which would place it closer to the small, northeastern caldera. The markedly smaller azimuth predicted by the triaxial ellispoid may possibly be explained by its large extent in EW direction compared to the other geometries. Combining the

elastic structure and the topography (CSSM–C2PC) reduced the azimuth compared to the values predicted by the elastic structure model (ESSM–E2PC), but the combined model (CSSM–C2PC) still predicts a larger value than the homogeneous model.

Considering the depth, pressure change, predicted azimuth, and tilt at GFUM, the models with one or two penny-shaped cracks (CPSC, C2PC) appear as the best fitting geometries out of the five tested. The source pressures of the two spheres (CSSM, CSLA) are unrealistically large and the predicted tilt is less than what was observed (Table 5). The single penny-shaped crack (CPSC) was the only geometry, which predicted tilt within the observational uncertainties, but the addition of a second, deeper magmatic body seems to be required by geochemical analyses and to explain post-eruptive deformation [Reverso et al. 2014; Haddadi et al. 2017]. Future studies should, especially if they use two interconnected magma bodies, consider more complex pressure-boundary conditions than the ones used in this study. Although all geometries tested could reproduce the observations of GFUM from 2011, the predicted deformation differs almost everywhere else and additional observation points should be able to further constrain the geometry of the deformation source. Lastly, it should be noted that the model parameters of the current study were found using essentially trial and error and that no parameter uncertainties were given since none of the datasets used as input for the model had estimates for the uncertainty either. Further studies using the current or a similar setup may be able to change this.

6 Conclusions

The models presented in this study help to better understand the influence of topography in a caldera-setting and crustal heterogeneity on surface deformation and to constrain source parameters of the deformation source at Grímsvötn and other volcanoes of complex crustal structure. The main conclusions are:

1. The elastic subsurface structure strongly influences both the surface deformation and the resulting model parameters. The dominating elements of the elastic structure are the 3D p-wave velocity model by Alfaro et al. [2007] and the relation between static and dynamic moduli based on laboratory estimates by Adelinet et al. [2010]. The topography has a limited effect on the model parameters, but still has visible effects on the surface deformation, especially the horizontal component. Similar effects may occur at other volcanoes, although the influence of each feature depends on the individual system.

2. Five deformation sources were tested in a model which combines topography and a 3D heterogeneous elastic subsurface structure. The source depths required to reproduce the coeruptive displacement from the 2011 eruption at Grímsvötn range between ca. 3–4.5 km below the surface with corresponding pressure changes typically between 8–70 MPa. These depths are significantly deeper than those found by previous geodetic studies. The best fitting geometry is either a single or two vertically stacked penny-shaped cracks.

3. We scaled the dynamic elastic moduli derived from seismic velocities with the lithostatic pressure to obtain large-scale variable estimates of the static elastic moduli, which are more appropriate to use for ground deformation than the typically higher, dynamic moduli. Applying a pressure-dependent relation between dynamic and static elastic moduli is new for volcano deformation models. The approach suggested here is, however, still a simplification of reality and subject to further studies.

Author Contributions

HG initially designed the study; models were set up and run by SG; SG produced all figures; SG and HG interpreted results; SG drafted the manuscript and HG edited; SG and HG worked on revisions.

Acknowledgements

We acknowledge the Institute of Earth Sciences at the University of Iceland for funding the COMSOL license used in this study. Parts of this study are based on SG's master thesis. Furthermore, parts of this study were covered by RANNÍS-grant No. 174377-051. The data for the timeseries of GFUM in Figure 1C–E are from the Icelandic Meteorological Office. We thank Bryndís Brandsdóttir for sharing the seismic velocity model and Eyjólfur Magnússon for sharing the bedrock topography data with us. We thank Freysteinn Sigmundsson for helpful discussions on the models and Magnús-Tumi Guðmundsson for sharing his knowledge about the Grímsvötn volcanic system in general and Grímsfjall in particular. We also thank Editor Jamie Farquharson and Reviewers Jean-Luc Got and James Hickey for comments that improved the initial manuscript.

Data Availability

Supporting information and models implemented in this study are available at https://doi.org/10.5281/zenodo.13981084.

Copyright Notice

References

Adelinet, M., J. Fortin, Y. Guéguen, A. Schubnel, and L. Geoffroy (2010). "Frequency and fluid effects on elastic properties of basalt: Experimental investigations". *Geophysical Research Letters* 37(2). DOI: 10.1029/2009GL041660.

Albino, F., V. Pinel, and F. Sigmundsson (2010). "Influence of surface load variations on eruption likelihood: application to two Icelandic subglacial volcanoes, Grímsvötn and Katla". *Geophysical Journal International* 181(3), pages 1510–1524. DOI: 10.1111/j.1365-246X.2010.04603.x.

Alfaro, R., B. Brandsdóttir, D. P. Rowlands, R. S. White, and M. T. Gudmundsson (2007). "Structure of the Grímsvötn central volcano under the Vatnajökull icecap, Iceland". *Geophysical Journal International* 168(2), pages 863–876. DOI: 10.1111/j.1365-246X.2006.03238.x.

Amelung, F., S. Jónsson, H. Zebker, and P. Segall (2000). "Widespread uplift and 'trapdoor'faulting on Galapagos volcanoes observed with radar interferometry". *Nature* 407(6807), pages 993–996. DOI: 10.1038/35039604.

Anderson, K. and P. Segall (2011). "Physics-based models of ground deformation and extrusion rate at effusively erupting volcanoes". *Journal of Geophysical Research: Solid Earth* 116(B7). DOI: 10.1029/2010JB007939.

Battaglia, M., P. F. Cervelli, and J. R. Murray (2013). "dMODELS: A MATLAB software package for modeling crustal deformation near active faults and volcanic centers". *Journal of Volcanology and Geothermal Research* 254, pages 1–4. DOI: 10.1016/j.jvolgeores.2012.12.018.

Björnsson, H. and P. Einarsson (1990). "Volcanoes beneath Vatnajökull, Iceland: Evidence from radio echo-sounding, earthquakes and jökulhlaups". *Jökull* 40, pages 147–168.

Björnsson, H. and F. Pálsson (2020). "Radio-echo soundings on Icelandic temperate glaciers: history of techniques and findings". *Annals of Glaciology* 61(81), pages 25–34. DOI: 10.1017/aog.2020.10.

Cashman, K. V., R. S. J. Sparks, and J. D. Blundy (2017). "Vertically extensive and unstable magmatic systems: A unified view of igneous processes". *Science* 355(6331), eaag3055. DOI: 10.1126/science.aag3055.

Cayol, V. and F. H. Cornet (1998). "Effects of topography on the interpretation of the deformation field of prominent volcanoes—Application to Etna". *Geophysical Research Letters* 25(11), pages 1979–1982. DOI: 10.1029/98GL51512.

Cheng, C. H. and D. H. Johnston (1981). "Dynamic and static moduli". *Geophysical Research Letters* 8(1), pages 39–42. DOI: 10.1029/GL008i001p00039.

Currenti, G., C. Del Negro, G. Ganci, and D. Scandura (2008). "3D numerical deformation model of the intrusive event forerunning the 2001 Etna eruption". *Physics of the Earth and Planetary Interiors* 168(1), pages 88–96. DOI: 10.1016/j.pepi.2008.05.004.

Currenti, G. and C. A. Williams (2014). "Numerical modeling of deformation and stress fields around a magma chamber: Constraints on failure conditions and rheology". *Physics of the Earth and Planetary Interiors* 226, pages 14–27. DOI: 10.1016/j.pepi.2013.11.003.

Darbyshire, F. A., I. Bjarnason, R. S. White, and Ó. G. Flóvenz (1998). "Crustal structure above the Iceland mantle plume imaged by the ICEMELT refraction profile". *Geophysical Journal International* 135(3), pages 1131–1149. DOI: 10.1046/j.1365-246X.1998.00701.x.

Dieterich, J. H. and R. W. Decker (1975). "Finite element modeling of surface deformation associated with volcanism". *Journal of Geophysical Research (1896-1977)* 80(29), pages 4094–4102. DOI: 10.1029/JB080i029p04094.

Eggertsson, G. H., J. E. Kendrick, J. Weaver, P. A. Wallace, J. E. Utley, J. D. Bedford, M. J. Allen, S. H. Markússon, R. H. Worden, D. R. Faulkner, and Y. Lavallée (2020). "Compaction of hyaloclastite from the active geothermal system at Krafla volcano, Iceland". *Geofluids* 2020. DOI: 10.1155/2020/3878503.

Einarsson, P. (2008). "Plate boundaries, rifts and transforms in Iceland". *Jökull* 58, pages 35–58.

Einarsson, P. and K. Sæmundsson (1987). "Earthquake Epicenters 1982-1985 and Volcanic Systems in Iceland: Upptok Jardskjalfta 1982-1985 og Eldstodvakerfi a Islandi". *in Í hlutarins edli*. Edited by T. I. Sigfusson. Reykjavik, Iceland: Menningarsjóður. [Map].

Eissa, E. and A. Kazi (1988). "Relation between static and dynamic Young's moduli of rocks". *International Journal of Rock Mechanics and Mining & Geomechanics Abstracts* 25(6).

Fjær, E. (2019). "Relations between static and dynamic moduli of sedimentary rocks". *Geophysical Prospecting* 67(1), pages 128–139. DOI: 10.1111/1365-2478.12711.

Folch, A. and J. Gottsmann (2006). "Faults and ground uplift at active calderas". *Geological Society, London, Special Publications* 269(1), pages 109–120. DOI: 10.1144/GSL.SP.2006.269.01.07.

Foroozan, R., D. Elsworth, B. Voight, and G. S. Mattioli (2010). "Dual reservoir structure at Soufrière Hills Volcano inferred from continuous GPS observations and heterogeneous elastic modeling". *Geophysical Research Letters* 37(19). DOI: 10.1029/2010GL042511.

Got, J.-L., D. Amitrano, I. Stefanou, E. Brothelande, and A. Peltier (2019). "Damage and Strain Localization Around a Pressurized Shallow-Level Magma Reservoir". *Journal of Geophysical Research: Solid Earth* 124(2), pages 1443–1458. DOI: 10.1029/2018JB016407.

Gottsmann, J., M. Flynn, and J. Hickey (2020). "The Transcrustal Magma Reservoir Beneath Soufrière Hills Volcano, Montserrat: Insights From 3-D Geodetic Inversions". *Geophysical Research Letters* 47(20), e2020GL089239. DOI: 10.1029/2020GL089239.

Grapenthin, R., F. Sigmundsson, H. Geirsson, T. Árnadóttir, and V. Pinel (2006). "Icelandic rhythmics: Annual modulation of land elevation and plate spreading by snow load". *Geophysical Research Letters* 33(24). DOI: 10.1029/2006GL028081.

Gudmundsson, A. (2012). "Magma chambers: Formation, local stresses, excess pressures, and compartments". *Journal of Volcanology and Geothermal Research* 237-238, pages 19–41. DOI: 10.1016/j.jvolgeores.2012.05.015.

Gudmundsson, M. T. (1989). "The Grímsvötn caldera, Vatnajökull: subglacial topography and structure of caldera infill". *Jökull* (39), pages 1–20.

Gudmundsson, M. T., H. Björnsson, and F. Pálsson (1995). "Changes in jökulhlaup sizes in Grímsvötn, Vatnajökull, Iceland, 1934-91, deduced from in-situ measurements of subglacial lake volume". *Journal of Glaciology* 41(138), pages 263–272. DOI: 10.3189/S0022143000016166.

Gudmundsson, M. T., K. Jónsdóttir, A. Hooper, E. P. Holohan, S. A. Halldórsson, B. G. Ófeigsson, S. Cesca, K. S. Vogfjörd, F. Sigmundsson, T. Högnadóttir, P. Einarsson, O. Sigmarsson, A. H. Jarosch, K. Jónasson, E. Magnússon, S. Hreinsdóttir, M. Bagnardi, M. M. Parks, V. Hjörleifsdóttir, F. Pálsson, T. R.

Walter, M. P. J. Schöpfer, S. Heimann, H. I. Reynolds, S. Dumont, E. Bali, G. H. Gudfinnsson, T. Dahm, M. J. Roberts, M. Hensch, J. M. C. Belart, K. Spaans, S. Jakobsson, G. B. Gudmundsson, H. M. Fridriksdóttir, V. Drouin, T. Dürig, G. Aðalgeirsdóttir, M. S. Riishuus, G. B. M. Pedersen, T. van Boeckel, B. Oddsson, M. A. Pfeffer, S. Barsotti, B. Bergsson, A. Donovan, M. R. Burton, and A. Aiuppa (2016). "Gradual caldera collapse at Bárdarbunga volcano, Iceland, regulated by lateral magma outflow". *Science* 353(6296), aaf8988. DOI: 10.1126/science.aaf8988.

Gudmundsson, M. T. and J. Milsom (1997). "Gravity and magnetic studies of the subglacial Grímsvötn volcano, Iceland: Implications for crustal and thermal structure". *Journal of Geophysical Research: Solid Earth* 102(B4), pages 7691–7704. DOI: 10.1029/96JB03808.

Gudmundsson, Ó. (2003). "The dense root of the Iceland crust". *Earth and Planetary Science Letters* 206(3), pages 427–440. DOI: 10.1016/S0012-821X(02)01110-X.

Haddadi, B., O. Sigmarsson, and G. Larsen (2017). "Magma storage beneath Grímsvötn volcano, Iceland, constrained by clinopyroxene-melt thermobarometry and volatiles in melt inclusions and groundmass glass". *Journal of Geophysical Research: Solid Earth* 122(9), pages 6984–6997. DOI: 10.1002/2017JB014067.

Haimson, B. C. and F. Rummel (1982). "Hydrofracturing stress measurements in the Iceland Research Drilling Project drill hole at Reydarfjordur, Iceland". *Journal of Geophysical Research: Solid Earth* 87(B8), pages 6631–6649. DOI: 10.1029/JB087iB08p06631.

Hautmann, S., J. Gottsmann, R. S. J. Sparks, G. S. Mattioli, I. S. Sacks, and M. H. Strutt (2010). "Effect of mechanical heterogeneity in arc crust on volcano deformation with application to Soufrière Hills Volcano, Montserrat, West Indies". *Journal of Geophysical Research: Solid Earth* 115(B9). DOI: 10.1029/2009JB006909.

Heap, M. J., M. V. sand F. Albino, J. Farquharson, E. Brothelande, F. Amelung, J.-L. Got, and P. Baud (2020). "Towards more realistic values of elastic moduli for volcano modelling". *Journal of Volcanology and Geothermal Research* 390, page 106684. DOI: 10.1016/j.jvolgeores.2019.106684.

Hickey, J., J. Gottsmann, and P. Mothes (2015). "Estimating volcanic deformation source parameters with a finite element inversion: The 2001–2002 unrest at Cotopaxi volcano, Ecuador". *Journal of Geophysical Research: Solid Earth* 120(3), pages 1473–1486. DOI: 10.1002/2014JB011731.

Hickey, J., J. Gottsmann, H. Nakamichi, and M. Iguchi (2016). "Thermomechanical controls on magma supply and volcanic deformation: application to Aira caldera, Japan". *Scientific reports* 6(1), page 32691. DOI: 10.1038/srep32691.

Hreinsdóttir, S., F. Sigmundsson, M. J. Roberts, H. Björnsson, R. Grapenthin, P. Arason, T. Árnadóttir, J. Hólmjárn, H. Geirsson, R. A. Bennet, M. T. Gudmundsson, B. Oddson, B. G. Ófeigsson, T. Villemin, T. Jónsson, E. Sturkell, Á. Höskuldsson, G. Larsen, T. Thordarson, and B. A. Óladóttir (2014). "Volcanic plume height correlated with magma-pressure change at Grímsvötn Volcano, Iceland". *Nature Geoscience* 7(3), pages 214–218. DOI: 10.1038/ngeo2044.

Johnson, J. H., M. P. Poland, K. R. Anderson, and J. Biggs (2019). "A Cautionary Tale of Topography and Tilt from Kilauea Caldera". *Geophysical Research Letters* 46(8), pages 4221–4229. DOI: 10.1029/2018GL081757.

Jónsson, S. (2012). "Tensile rock mass strength estimated using InSAR". *Geophysical Research Letters* 39(21). DOI: 10.1029/2012GL053309.

Liao, Y., S. A. Soule, and M. Jones (2018). "On the Mechanical Effects of Poroelastic Crystal Mush in Classical Magma Chamber Models". *Journal of Geophysical Research: Solid Earth* 123(11), pages 9376–9406. DOI: 10.1029/2018JB015985.

Link, H. (1968). "Zum Verhältnis seismisch und statisch ermittelter Elastizitätsmoduln von Fels (On the correlation of seismically and statically determined moduli of elasticity of rock masses)". *Aktuelle Probleme der Geomechanik und Deren theoretische Anwendung/Acute Problems of Geomechanics and Their Theoretical Applications*. Springer, pages 90–110.

Lisowski, M. (2007). *Volcano Deformation: Geodetic monitoring techniques*. Edited by D. Dzurision. Springer-Verlag Berlin Heidelberg New York, pages 279–304.

Magnússon, E. (2008). "Glacier hydraulics explored by means of SAR-interferometry". PhD thesis. Leopold-Franzens-Universität.

Masterlark, T. (2007). "Magma intrusion and deformation predictions: Sensitivities to the Mogi assumptions". *Journal of Geophysical Research: Solid Earth* 112(B6). DOI: 10.1029/2006JB004860.

McTigue, D. F. (1987). "Elastic stress and deformation near a finite spherical magma body: Resolution of the point source paradox". *Journal of Geophysical Research: Solid Earth* 92(B12), pages 12931–12940. DOI: 10.1029/JB092iB12p12931.

Mogi, K. (1958). "Relations between the eruptions of various volcanoes and the deformations of the ground surfaces around them". *Bulletin of the Earthquake Research Institute of the University of Tokyo* 36, pages 99–134.

Poppe, S., C. Wauthier, and K. Fontijn (2024). "Inversions of Surface Displacements in Scaled Experiments of Analog Magma Intrusion". *Geophysical Research Letters* 51(8), e2023GL106805. DOI: 10.1029/2023GL106805.

Reverso, T., J. Vandemeulebrouck, F. Jouanne, V. Pinel, T. Villemin, E. Sturkell, and P. Bascou (2014). "A two-magma chamber model as a source of deformation at Grímsvötn Volcano, Iceland". *Journal of Geophysical Research: Solid Earth* 119(6), pages 4666–4683. DOI: 10.1002/2013JB010569.

Rivalta, E. and P. Segall (2008). "Magma compressibility and the missing source for some dike intrusions". *Geophysical Research Letters* 35(4). DOI: 10.1029/2007GL032521.

Sigmundsson, F., P. Einarsson, Á. R. Hjartardóttir, V. Drouin, K. Jónsdóttir, T. Árnadóttir, H. Geirsson, S. Hreinsdóttir, S. Li, and B. G. Ófeigsson (2020a). "Geodynamics of Iceland and the signatures of plate spreading". *Journal of Volcanology and Geothermal Research* 391, page 106436. DOI: 10.1016/j.jvolgeores.2018.08.014.

Sigmundsson, F., M. Parks, H. Geirsson, A. Hooper, V. Drouin, K. S. Vogfjörd, B. G. Ófeigsson, S. H. M. Greiner, Y. Yang, C. Lanzi, G. P. De Pascale, K. Jónsdóttir, S. Hreinsdóttir, V. Tolpekin, H. M. Fridriksdóttir, P. Einarsson, and S. Barsotti (2024). "Fracturing and tectonic stress drive ultrarapid magma flow into dikes". *Science* 383(6688), pages 1228–1235. DOI: 10.1126/science.adn2838.

Sigmundsson, F., M. Parks, A. Hooper, H. Geirsson, K. S. Vogfjörd, V. Drouin, B. G. Ófeigsson, S. Hreinsdóttir, S. Hjaltadóttir, K. Jónsdóttir, P. Einarsson, S. Barsotti, J. Horálek, and T. Ágústsdóttir (2022). "Deformation and seismicity decline before the 2021 Fagradalsfjall eruption". *Nature* 609(7927), pages 523–528. DOI: 10.1038/s41586-022-05083-4.

Sigmundsson, F., V. Pinel, R. Grapenthin, A. Hooper, S. A. Halldórsson, P. Einarsson, B. G. Ófeigsson, E. R. Heimisson, K. Jónsdóttir, M. T. Gudmundsson, et al. (2020b). "Unexpected large eruptions from buoyant magma bodies within viscoelastic crust". *Nature communications* 11(1), pages 1–11. DOI: 10.1038/s41467-020-16054-6.

Simmons, G. and W. F. Brace (1965). "Comparison of static and dynamic measurements of compressibility of rocks". *Journal of Geophysical Research (1896-1977)* 70(22), pages 5649–5656. DOI: 10.1029/JZ070i022p05649.

Sturkell, E., P. Einarsson, F. Sigmundsson, S. Hreinsdóttir, and H. Geirsson (2003). "Deformation of Grímsvötn volcano, Iceland: 1998 eruption and subsequent inflation". *Geophysical Research Letters* 30(4). DOI: 10.1029/2002GL016460.

Thordarson, T. and G. Larsen (2007). "Volcanism in Iceland in historical time: Volcano types, eruption styles and eruptive history". *Journal of Geodynamics* 43(1). Hotspot Iceland, pages 118–152. DOI: 10.1016/j.jog.2006.09.005.

Thordarson, T. and S. Self (1993). "The Laki (Skaftár Fires) and Grímsvötn eruptions in 1783–1785". *Bulletin of Volcanology* 55(4), pages 233–263. DOI: 10.1007/BF00624353.

Trasatti, E., C. Giunchi, and M. Bonafede (2003). "Effects of topography and rheological layering on ground deformation in volcanic regions". *Journal of Volcanology and Geothermal Research* 122(1), pages 89–110. DOI: 10.1016/S0377-0273(02)00473-0.

Trasatti, E., C. Giunchi, and M. Bonafede (2005). "Structural and rheological constraints on source depth and overpressure estimates at the Campi Flegrei caldera, Italy". *Journal of Volcanology and Geothermal Research* 144(1). The Tectonics and Physics of Volcanoes, pages 105–118. DOI: 10.1016/j.jvolgeores.2004.11.019.

Vogfjörd, K. S., S. S. Jakobsdóttir, G. B. Gudmundsson, M. J. Roberts, K. Ágústsson, T. Arason, H. Geirsson, S. Karlsdóttir, S. Hjaltadóttir, U. Ólafsdóttir, B. Thorbjarnardóttir, G. Hafsteinsson, H. Sveinbjörnsson, R. Stefánsson, and T. V. Jónsson (2005). "Forecasting and monitoring a subglacial eruption in Iceland". *Eos, Transactions American Geophysical Union* 86(26), pages 245–248. DOI: 10.1029/2005EO260001.

Watton, T., D. Jerram, T. Thordarson, and R. Davies (2013). "Three-dimensional lithofacies variations in hyaloclastite deposits". *Journal of Volcanology and Geothermal Research* 250, pages 19–33. DOI: 10.1016/j.jvolgeores.2012.10.011.

Wauthier, C., V. Cayol, F. Kervyn, and N. d'Oreye (2012). "Magma sources involved in the 2002 Nyiragongo eruption, as inferred from an InSAR analysis". *Journal of Geophysical Research: Solid Earth* 117(B5). DOI: 10.1029/2011JB008257.

Werner, R. and H. Schmincke (1999). "Englacial vs lacustrine origin of volcanic table mountains: evidence from Iceland". *Bulletin of Volcanology* 60(5), pages 335–354. DOI: 10.1007/s004450050237.

Williams, C. A. and G. Wadge (1998). "The effects of topography on magma chamber deformation models: Application to Mt. Etna and radar interferometry". *Geophysical Research Letters* 25(10), pages 1549–1552. DOI: 10.1029/98GL01136.

Zhang, Y., Y. Gu, H. Zhou, and L. Yang (2024). "Extracting static elastic moduli of rock through elastic wave velocities". *Acta Geophysica* 72(2), pages 915–931. DOI: 10.1007/s11600-023-01139-9.